Loschmidt amplitude spectrum in dynamical quantum phase transitions

Cheuk Yiu Wong and Wing Chi Yu*
Department of Physics, City University of Hong Kong, Kowloon, Hong Kong

(Received 30 November 2021; revised 6 March 2022; accepted 10 May 2022; published 26 May 2022)

Dynamical quantum phase transitions (DQPTs) are criticalities in the time evolution of quantum systems and their existence has been theoretically predicted and experimentally observed. However, how the system behaves in the vicinity of DQPT and its connection to physical observables remains an open question. In this work, we introduce the concept of the Loschmidt amplitude spectrum (LAS), which extends the Loscmidt amplitude - the detector of the transition - by considering the overlap of the initial state to all the eigenstates of the prequench Hamiltonian. By analyzing the LAS in the integrable transverse-field Ising model, we find that the system undergoes a population redistribution in the momentum space across DQPT. In the quasiparticle picture, collective excitations around lower-half k modes become dominant when the system approaches DQPT. The LAS is also applicable to study the dynamics of nonintegrable models where we have investigated the Ising model with next-nearest-neighbor interactions as an example. The time evolution of the system's magnetization is found to be connected to the products of the LAS and there exists a simultaneous overlap of the time-evolved state to pairs of eigenstates of the prequnech Hamiltonian that possess spin configurations of negative magnetization. Our findings provide a better understanding of the characteristics of the out-of-equilibrium system around DQPT.

DOI: 10.1103/PhysRevB.105.174307

I. INTRODUCTION

The research on dynamical quantum phase transitions (DQPTs) has been thriving, both in experimental [1–5] and theoretical researches [6–49], among condensed matter physicists. On the one hand, quantum simulators have allowed access to the real-time dynamics of quantum systems in experiments [1–5,50–60], among which detection of DQPT was found possible [1–5]. On the other hand, theoretical studies of DQPTs have advanced our understanding of nonequilibrium physics in quantum many-body systems, among which may lead to potential applications in quantum computing [61,62].

The central study of DQPTs relies on the concept of *Loschmidt amplitude* (LA), which measures the overlap of the time-evolving system onto its initial state, i.e.,

$$\mathcal{G}_0(t) = \langle \psi_0(g_i)|e^{-iH(g_f)t}|\psi_0(g_i)\rangle, \tag{1}$$

where $|\psi_0(g_i)\rangle$ is the ground state of the Hamiltonian $H(g_i)$ and $H(g_f)$ is the quenched Hamiltonian. DQPTs are defined by the zeros in the *Loschmidt echo* (LE) $\mathcal{L}_0(t) = |\mathcal{G}_0(t)|^2$ or the nonanalyticities in its rate function $\lambda_0(t) = -\lim_{N\to\infty} \ln \mathcal{L}_0(t)/N$, where N is the system size [6]. They are analogous to the zeros in the partition function and the nonanalyticities in the free energy in equilibrium phase transitions, and therefore $\lambda_0(t)$ is also called the dynamical free energy. Previous studies show that in most cases, DQPTs occur when the system is quenched across its equilibrium critical point g_c [63,64] though there are exceptions found in, for examples, Refs. [8,9,49]. The above are in fact type-II DQPTs. There are also type-I DQPTs describing the order parameter in late time staying finite or vanishing in different dynamical phases [10,11,65,66]. A recent study has shown that the two types of DQPTs are actually related in the long-range transverse field Ising model [10]. In this paper, we will focus on type-II DQPTs.

In spite of the wealth of literature successfully arguing the presence of DQPT in different models [63,64], the question of how the system behaves in the vicinity of DQPT is yet to be addressed. Various physical quantities have been investigated in attempt to unveil the system's characteristics around DQPT. For examples, nonanalytical behaviors are found in the correlation matrices, and crossings and degeneracy in the entanglement spectrum are observed at DQPTs [12–16,31]. It is also showed that there exists correspondence between DQPT and the systems' equilibrium order parameter in some models. For instance, the magnetization in the transverse-field Ising model and its variations was found both analytically and experimentally switching between positive and negative regime at the critical times [2,6,17–19], providing a more physical linkage of DQPTs to physical observables. Dynamical topological order parameters are also introduced to study the topological properties of DQPTs. The Pancharantnam geometric phase in the momentum space is found to exhibit a discontinuous jump at critical times [1,4,20,21,37] in noninteracting models. Another dynamical topological order parameter defined by the time-ordered two-point Green's function, which is applicable for interacting systems, is also found to have discontinuity across the DQPT [22].

In this work, we attempt to provide insights to the above-mentioned open question. Motivated by the observation that the dynamics of a quantum system shall depend on the whole spectrum of the Hamiltonian, we extend the conventional definition of the LA in Eq. (1), which just takes into account

*wingcyu@cityu.edu.hk

the overlaps onto the ground state, to the overlaps onto the excited states. We name the extension the *Loschmidt amplitude spectrum* (LAS) of a system. The LAS does not require empirical knowledge of the order parameters, rather one only needs to retrieve the spectrum of the system concerned, which is already computed upon computing the dynamical time-evolution of the initial state. The LAS is a conceptually lighter alternative to access the dynamic profile of a general condensed matter system.

To show how one uses the LAS in practice, we applied the LAS to investigate the dynamics in both integrable and nonintegrable models. We found that the integrable one-dimensional (1D) transverse-field Ising model experiences temporary population migration in the momentum space around DQPTs. Namely the quench triggers excitation concentrated on the middle range of the allowed k values in the momentum space, whereas at DQPT the excitation shifts downward to the lower-half range. We also examined the LAS for various quench parameters, and confirmed that nonanalyticities persist in LAS for typical quenches such as quenches within one phase. On the other hand, the nonintegrable 1D axial next-nearest-neighbor Ising (ANNNI) model exhibits substantial drop of magnetization when quenched from paramagnetic (PM) phase to ferromagnetic (FM) phase, and we found that the drop can be attributed to the simultaneous finite overlap between the time-evolved state and the eigenstate pairs with negative spin magnetization of the prequenched Hamiltonian.

The paper is organized as the following: The definition of LAS is presented in Sec. II. The results for 1D transverse-field Ising model, including the analytical expression of LAS in momentum space and the numerical calculations of different quenches, are given in Sec. III. In Sec. IV, the LAS of the 1D ANNNI model and its relation to the magnetization of the system are investigated. Finally, a conclusion is given in Sec. V.

II. LAS

Consider a system described by the Hamiltonian $H(g)$ such that $H(g)|\psi_n(g)\rangle = E_n(g)|\psi_n(g)\rangle$, where $|\psi_n(g)\rangle$ is the nth eigenstate of the Hamiltonian with the corresponding eigenenergy $E_n(g)$. Unless otherwise specified, we prepare the initial state of the system to be the ground state of $H(g_i)$, and quench the system with $H(g_f)$ at time $t = 0$. The LAS is defined by

$$\mathcal{G}_n(t) = \langle\psi_n(g_i)|e^{-iH(g_f)t}|\psi_0(g_i)\rangle, \tag{2}$$

and the respective rate function spectrum

$$\lambda_n(t) = \lim_{N\to\infty} -\frac{1}{N}\log[\mathcal{L}_n(t)], \tag{3}$$

where $\mathcal{L}_n(t) = |\mathcal{G}_n(t)|^2$ is the LE spectrum. Throughout the whole paper, we use Loschmidt amplitude/echo/rate spectrum (LAS/LES/LRS) interchangeably.

For a general n, the LAS measures the overlap between the time-evolving state and the nth eigenstate of the initial Hamiltonian. It quantifies how much the quenched state is scattered into an excited state of the initial Hamiltonian. A similar quantity that measures the overlap between the time-evolving state with the final Hamiltonian's eigenstates has also been investigated to understand the quench dynamics in some analytically solvable topological models [67]. Here we focus on the overlap with the eigenstates of the initial Hamiltonian, which can be a many-body wave function in general, as a natural extension to the original definition of LA. The quantity in Eq. (2) represents the first column of the evolution operator matrix $e^{-iH(g_f)t}$ expanded in the eigenstates of $H(g_i)$ while the conventional definition of LA in Eq. (1) only captures the first diagonal element of the matrix. Therefore, we expect more information about the dynamics of the system to be encoded in the LAS. By analyzing the LAS and the corresponding rate function spectrum, insights into the characteristics of the quantum state around the DQPT can be drawn. A similar quantity has also been studied in the context of fidelity spectrum in equilibrium QPTs [68] and many-body localizations [69]. Here we extend the study to a time-dependent case and demonstrate the idea using the 1D transverse-field Ising model and the ANNNI model.

III. 1D TRANSVERSE-FIELD ISING MODEL

The Hamiltonian of the transverse-field Ising model is given by

$$H(g) = -J\sum_{j=1}^{N}\left(\sigma_j^x\sigma_{j+1}^x + g\sigma_j^z\right), \tag{4}$$

where J is the Ising coupling, g represents the external magnetic field strength, and σ_j^α ($\alpha = x, y, z$) are the Pauli matrices of site j. The periodic boundary condition is adopted. Below we set $J = 1$ for convenience.

The model is first transformed by the Jordan-Wigner transformation $\sigma_j^\pm = \exp[\pm i\pi\sum_{n=1}^{j-1}c_n^\dagger c_n]c_j$ and $\sigma_j^z = 1 - 2c_j^\dagger c_j$ to a spinless fermionic model, followed by a Fourier transformation $c_j = (1/\sqrt{N})\sum_k e^{-ikj}c_k$, where the Hamiltonian becomes

$$H(g) = \sum_k[(2g - 2\cos k)c_k^\dagger c_k + i\sin k(c_k^\dagger c_{-k}^\dagger - c_{-k}c_k)] - Ng, \tag{5}$$

with $c_k(c_k^\dagger)$ being a set of fermionic annihilation (creation) operators with $k = \pm\pi/N, \pm 3\pi/N, \ldots, \pm(N-1)\pi/N$ for even N in the even-parity subspace [70].

The quadratic Hamiltonian in Eq. (5) can be diagonalized by performing Bogoliubov transformation, namely, $c_k = u_k(g)\beta_k + iv_k(g)\beta_{-k}^\dagger$, where $u_k(g) = \cos(\theta_k(g))$ and $v_k(g) = \sin(\theta_k(g))$. The $\theta_k(g) \in [0, \pi/2]$ is called the Bogoliubov angle satisfying the condition $\tan(2\theta_k) = (\sin k)/(\cos k - g)$. The resulting Hamiltonian is

$$H(g) = \sum_{k>0}\varepsilon_k(g)(\beta_k^\dagger\beta_k - \beta_{-k}\beta_{-k}^\dagger), \tag{6}$$

with $\varepsilon_k(g) = 2\sqrt{(\cos k - g)^2 + \sin^2 k}$. The ground state is the vacuum state $|0(g)\rangle$ such that $\beta_k|0(g)\rangle = 0$ for all k. The excited states can be generated by creating pairs of opposite-momentum quasiparticles in different k modes on the vacuum state. A quantum phase transition takes place when the magnetic field changes across the critical point $g_c = 1$. The system

transforms from a FM phase to a PM phase when g increases from below g_c and vice versa.

The LA of the system for a sudden quench $g_i \to g_f$ has an analytical expression derived by Silva [71]: Let η_k and γ_k be the eigenmodes of Hamiltonian $H(g_i)$ and $H(g_f)$, respectively; one can easily write the transformation in-between as $\eta_k = U_k\gamma_k - iV_k\gamma_{-k}^\dagger$ with

$$\begin{aligned} U_k &= u_k(g_i)u_k(g_f) + v_k(g_i)v_k(g_f) \\ V_k &= u_k(g_i)v_k(g_f) - v_k(g_i)u_k(g_f). \end{aligned} \tag{7}$$

Thus the LA is given by

$$\begin{aligned} \mathcal{G}_0(t) = \frac{e^{-iE_0(g_f)t}}{\mathcal{N}^2}\langle 0(g_f)|[e^{-i\sum_{k>0}\frac{V_k}{U_k}\gamma_{-k}\gamma_k} \\ \times e^{i\sum_{k>0}\frac{V_k}{U_k}e^{-i2\varepsilon_k(g_f)t}\gamma_k^\dagger\gamma_{-k}^\dagger}]|0(g_f)\rangle, \end{aligned} \tag{8}$$

where $E_0(g_f)$ is the ground-state energy of $H(g_f)$ and $\mathcal{N}$ is the normalization factor.

The *ground-state* rate function can be calculated as

$$\lambda_0(t) \sim -\frac{1}{N}\sum_{k>0}\ln\left[1 + T_k^4 + 2T_k^2\cos(2\varepsilon_k(g_f)t)\right], \tag{9}$$

where $T_k = V_k/U_k = \tan(\phi_k)$ with $\phi_k = \theta_k(g_i) - \theta_k(g_f)$. Note that we have ignored an irrelevant constant term. Using Eq. (2), we obtain the LAS

$$\begin{aligned} \mathcal{G}_n(t) = \frac{e^{-iE_n(g_f)t}}{\mathcal{N}^2}\prod_{k'}[2T_{k'}\sin(\varepsilon_{k'}(g_f)t)e^{-i\varepsilon_{k'}(g_f)t}] \\ \times \prod_{k\neq k'>0}\left(1 + T_k^2 e^{-i2\varepsilon_k(g_f)t}\right), \end{aligned} \tag{10}$$

where the k' product includes all occupied k states; $E_n(g_f)$ is the energy of the corresponding excited state. With the expression above, we can compute the LRS easily,

$$\begin{aligned} \lambda_n(t) \sim -\frac{1}{N}\Bigg\{\sum_{k'}\ln\left[2T_{k'}^2(1-\cos(2\varepsilon_{k'}(g_f)t))\right] \\ + \sum_{k\neq k'>0}\ln\left[1 + T_k^4 + 2T_k^2\cos(2\varepsilon_k(g_f)t)\right]\Bigg\}. \end{aligned} \tag{11}$$

Comparing Eq. (11) with Eq. (9), they are similar to each other but the former contains an extra term $\sum_{k'}\Lambda_{k'}(t)$, where

$$\Lambda_{k'}(t) = -\frac{1}{N}\ln\left[2T_{k'}^2(1-\cos(2\varepsilon_{k'}(g_f)t))\right]. \tag{12}$$

Further to the LAS, one can generalize the concept to derive an analytical expression of the overlap between the time-evolving mth eigenstate and the nth eigenstate, namely,

$$\mathcal{G}_{nm}(t) = \langle\psi_n(g_i)|e^{-iH(g_f)t}|\psi_m(g_i)\rangle. \tag{13}$$

If resolved in Bogoliubov eigenbasis one obtains two distinct forms. The first is the diagonal terms where $m = n$,

$$\begin{aligned} \mathcal{G}_{nn}(t) = \frac{e^{-iE_0(g_f)t}}{\mathcal{N}^2}\prod_{k'}\left(T_{k'}^2 + e^{-i2\varepsilon_{k'}(g_f)t}\right) \\ \times \prod_{k\neq k'>0}\left(1 + T_k^2 e^{-i2\varepsilon_k(g_f)t}\right), \end{aligned} \tag{14}$$

where it gives the exact same LE and in turn LR as that for the ground state. The other form corresponds to the case when $m \neq n$ and is given by

$$\begin{aligned} \mathcal{G}_{nm}(t) = \mathcal{A}(t)\prod_{k'}[iV_{k'}(U_{k'} + V_{k'}T_{k'})(1 - e^{-i2\varepsilon_{k'}(g_f)t})] \\ \times \prod_{k\neq k'>0}\left(1 + T_k^2 e^{-i2\varepsilon_k(g_f)t}\right), \end{aligned} \tag{15}$$

where $\mathcal{A}(t) = \frac{e^{-iE_0(g_f)t}}{\mathcal{N}^2}$ is the insignificant prefactor. One can show that the corresponding LE reduces to the previously solved LES and thus the same rate function as Eq. (11). In other words, we expect that the LAS will be the same if we take the excited state as the initial state. In this paper, we would focus on the analysis of $m = 0$ case where the initial state is taken as the ground state.

The term $\Lambda_{k'}$ becomes nonanalytic when the argument of the logarithmic function is zero. The associated "critical time" is given by

$$t_p(k', g_f) = \frac{p\pi}{\varepsilon_{k'}(g_f)} \quad p = 1, 2, 3, \ldots, \tag{16}$$

which depends on the values of k' and g_f. For a general excited state, since k's are independent, the critical times in the LRS will be determined by all the k' modes in the excited state and their associated critical times given by Eq. (16). In fact, in the complex time plane, one easily realizes that the zeros of $\mathcal{G}_n(z)$, where $z \in \mathbb{C}$, are all lying on the imaginary time axis with a magnitude equal to $t_p(k', g_f)$. This implies that the nonanalyticities of LRs for excited states are insensitive to system size and they persist in large systems, unlike the case for ground-state rate function where it was shown in Ref. [6] that the Fisher zeros cross the imaginary time axis at thermodynamic limit. However, one shall not simply analogize the LAS defined in Eq. (2) for $n \neq 0$ to partition function in statistical mechanics.

Figure 1 shows the plot of the critical time in Eq. (16) versus k', which also represents the case of single mode excitation. As expected, critical time t_p decreases as k' increases. Note that an obvious horizontal "line" crosses around the middle of the graph. This refers to the discontinuity of $\lambda_n(t)$ against $\phi_{k'}$, where the Bogoliubov angle difference $\phi_{k'}$ jumps from strictly positive to strictly negative as k' increases, making the log function drop abruptly in magnitude and causing the large gap.

The $\Lambda_{k'}(t)$ alone has a neat property when we concern large systems. A simple analysis shows the vanishing of the term, namely, $|\Lambda_{k'}(t)| \lessapprox \ln(N)/N$ for k' close to $0, \pi$ and thus $|\Lambda_{k'}(t)| \to 0$ in the thermodynamic limit. It also holds true for a general allowed value of k' as suggested from finite size analysis of our numerical results. Consequentially, the rate function for excited states with only a few occupied

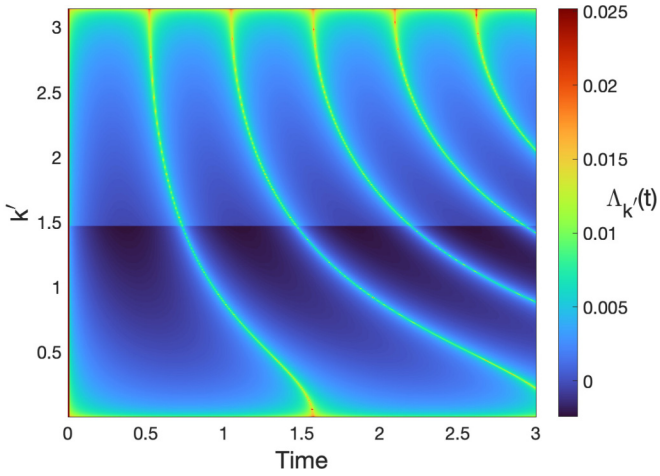

FIG. 1. Color map of $\Lambda_{k'}(t)$ in the LRS from an $N = 1000$ system quenched from $g = 0.1$ to 2. The nonanalytic peaks in $\Lambda_{k'}(t)$ become more evenly separated and denser in time as k' increases.

momentum states would behave similarly to the ground-state quantity during quenching, i.e., a large main peak equivalent to the ground-state nonanalyticity, except some small spikes can be seen along at times in Eq. (16) given by $\Lambda_{k'}(t)$.

On the other hand, the growth of the rate functions for higher excited states starts to behave differently and becomes more dramatic. The vanishing of $\Lambda_{k'}(t)$ does not apply to states with multimode excitation [72]. Figure 2

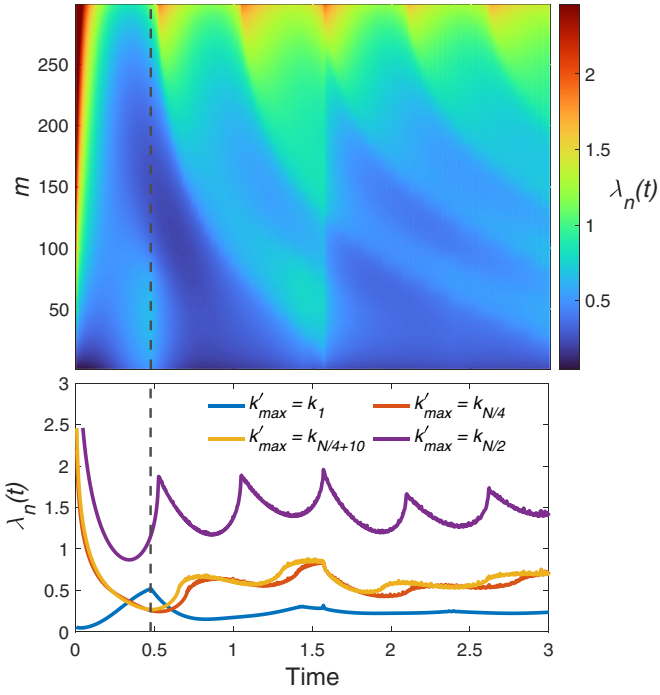

FIG. 2. (Top) Variation of LRS for excited states of the form $\prod_{k'=k_1}^{k'_{\max}} \eta^\dagger_{k'}\eta^\dagger_{-k'}|0(g_i)\rangle$, where $k_m = (2m-1)\pi/N$ with $m = 1, 2, \ldots, N/2$. (Bottom) Same quantities as the top panel with four specific values of $k'_{\max}$. The $N = 300$ system is quenched from $g = 0.1$ to 2. The dashed black lines indicate the first critical time in the ground-state rate function.

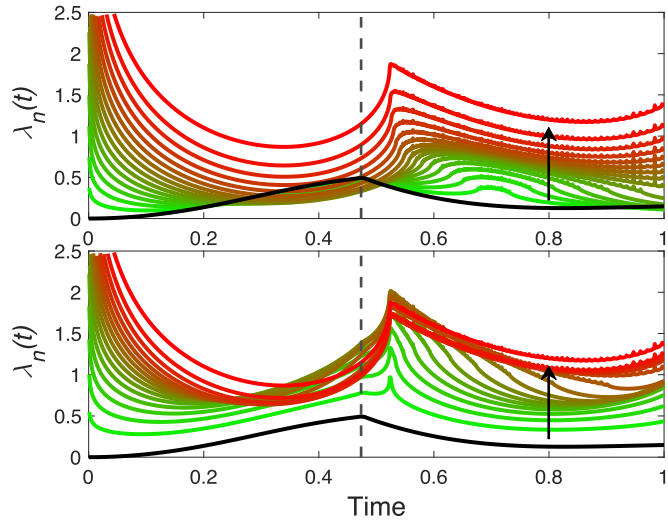

FIG. 3. The rate functions for the excited states of the form $\prod_{k'=k_{N/4-m}}^{k_{N/4+m+1}} \eta^\dagger_{k'}\eta^\dagger_{-k'}|0(g_i)\rangle$ with $m = 0, 1, 2, \ldots, N/4-1$ (top) and $\prod_{k'=k_{N/2-m'}}^{k_{N/2}} \eta^\dagger_{k'}\eta^\dagger_{-k'}|0(g_i)\rangle$ with $m' = 0, 1, 2, \ldots, N/2-1$ (bottom) of an $N = 300$ system quenched from $g = 0.1$ to 2.0. The black curve represents the ground-state Loschmidt rate with the dashed line indicating the first critical time, and the black arrow shows the direction of increasing m.

illustrates the trend of the rate functions for $|\psi_n(g_i)\rangle = \prod_{k'=\pi/N}^{k'_{\max}} \eta^\dagger_{k'}\eta^\dagger_{-k'}|0(g_i)\rangle$, where the product is taken over all occupied k modes for a quench across the equilibrium critical point. Comparing the rate functions at the ground-state critical time, we can see the turning from nonanalytical peaks to smooth valleys and then rising again to sharper peaks as we go up along the black dashed line. The valleys in rate functions correspond to the high probability of the overlap of the time-evolving state to the respective excited states. This suggests that the system is driven to a combination of states with mode excitation concentrating on the lower-half range at the DQPT when the system is quenched across the equilibrium critical point.

A further diagnosis of the spectrum is presented in Fig. 3, where we explore higher excited states with excitations in the middle range of the k spectrum and excitations starting from the highest k, respectively. Overall the quenched system would barely stay in highly excited states and the excitations occur mainly in the middle or low k modes during the dynamical evolution, as seen from Fig. 2 and Fig. 3. Notice, however, that we only show the dynamic responses around the first critical time as long-term dynamics are out of the scope of this paper.

Integrating the details shown previously, we suggest a physical description of the system's dynamics around the first critical time along with the aid of a schematic diagram in Fig. 4 as follows: The key concept is to realize that the diagonalized Hamiltonian in Eq. (6) represents a system of N two-level harmonic oscillators with independent momentum. The initial vacuum state refers to all the quasiparticles occupying the lower level. Once the system is being quenched, quasiparticles with momentum around the middle range of k spectrum (i.e., $k \sim \pi/2$) are excited to the upper level.

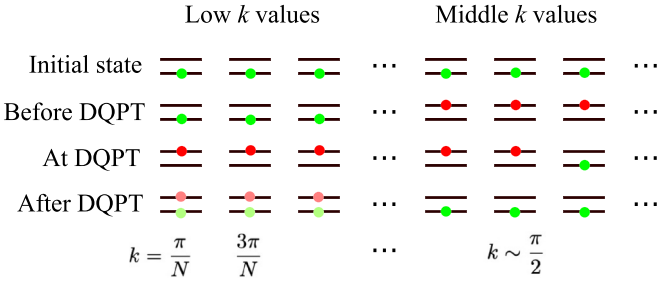

FIG. 4. Schematic diagram of the DQPTs of 1D TFIM in the diagonalized space. The dynamics of quench around DQPT can be represented as a series of excitations among the two-level systems. The green and red dots correspond to the relaxed and excited quasiparticles, respectively. The faded color dots represent a superposition of relaxed and excited quasiparticles at low k values beyond the critical time. Note that the quantum state of the system around the critical time is not only the state shown in the image but also a superposition of similar states. Subsequently the system would relax starting from the high k modes.

At DQPT, they drop to lower levels and are followed by excitation of k modes at lower-half k values. At later times, all the excited modes will gradually relax and return back to lower level. This occupation shift is when DQPTs occur. This phenomenon also occurs in DQPTs where the quench does not cross any underlying transition points in the XY model [23]. A brief discussion of the LAS of the XY model is given in the Supplemental Material [72].

The general quench dynamics for TFIM are also studied. Figure 5 shows the rate functions for $|\psi_n(g_i)\rangle$ being the

(1) ground state $|0(g_i)\rangle$;
(2) one-mode excited-state $\eta^\dagger_{k'}\eta^\dagger_{-k'}|0(g_i)\rangle$;
(3) lower-half excited-state $\prod_{k'=k_1}^{k_{N/4}} \eta^\dagger_{k'}\eta^\dagger_{-k'}|0(g_i)\rangle$;
(4) fully excited-state $\prod_{k'=k_1}^{k_{N/2}} \eta^\dagger_{k'}\eta^\dagger_{-k'}|0(g_i)\rangle$,

where $k_m = (2m-1)\pi/N$ for various quench parameters. There are obvious distinctions in the four cases. Figures 5(a) and 5(b) show a divergence in the critical time (as indicated by the bright lines) at $g = 1$, the equilibrium critical point separating the FM and PM phases. For the one-mode excited-state LR in Fig. 5(b), critical lines appear in places where they are absent in the ground-state rate function. In addition, forward and backward quenches are fairly symmetric in cases (a) and (b), whereas for higher excited states in cases (c) and (d), this symmetry is broken, and the behavior of LRS becomes more dramatic that the critical boundary starts to blur and kinks pass through the boundary. For the higher excited states, nonanalyticities are observed in the LRS for quenches within the same phase whereas the ground-state rate function goes smoothly as expected. The higher the excited state the denser the nonanalyticites in the LRS it possesses. It is still unclear whether these nonanalyticities that occurred in LAS satisfy the conditions to be a valid phase transition and it would be an interesting topic for further studies.

IV. 1D ANNNI MODEL

A variation of the quantum Ising model, also known as the ANNNI model, has also been shown to have exhibited DQPTs, and the next-nearest-neighbor interaction will further alter the characteristics of DQPT [38–41]. Here we provide a different point of view from the LAS to explain the dynamically critical phenomenon of the system. The Hamiltonian of ANNNI model is given by

$$H(\Delta, g) = -J\sum_{j=1}^{N}\left(\sigma_j^x\sigma_{j+1}^x + \Delta\sigma_j^x\sigma_{j+2}^x + g\sigma_j^z\right), \qquad (17)$$

with Δ controlling the next-nearest-neighbor interaction strength. When $\Delta = 0$, the model is reduced to the quantum Ising model in Eq. (4), where it can be diagonalized and quasiparticle picture interpretation applies. There are attempts to approximate transformation to retain the quasiparticle picture using mean-field Jordan-Wigner transformation [40]. Nonetheless, this work would present the numerical findings. The equilibrium ground-state phase diagram

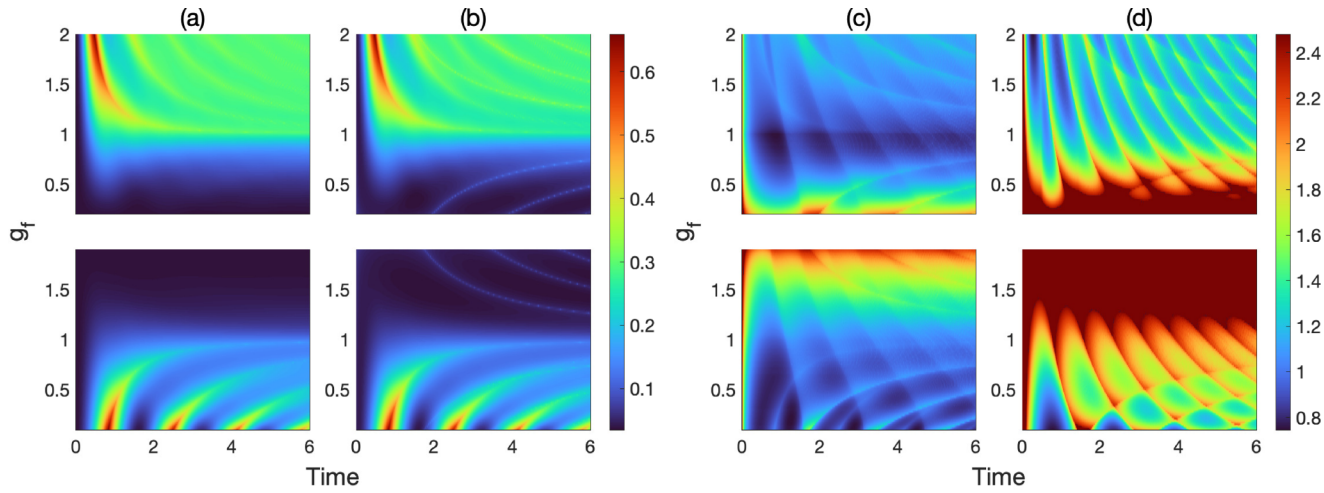

FIG. 5. LRS with various final parameters, namely, $g_i = 0.1 \to g_f$ from 0.2 to 2 for forward quench (top) and $g_i = 2 \to g_f$ from 1.9 to 0.1 for backward quench (bottom) for (a) ground state, (b) single-mode excited state, (c) lower-half excited state, and (d) fully occupied excited state. Colors represent the intensity of $\lambda_n(t)$.

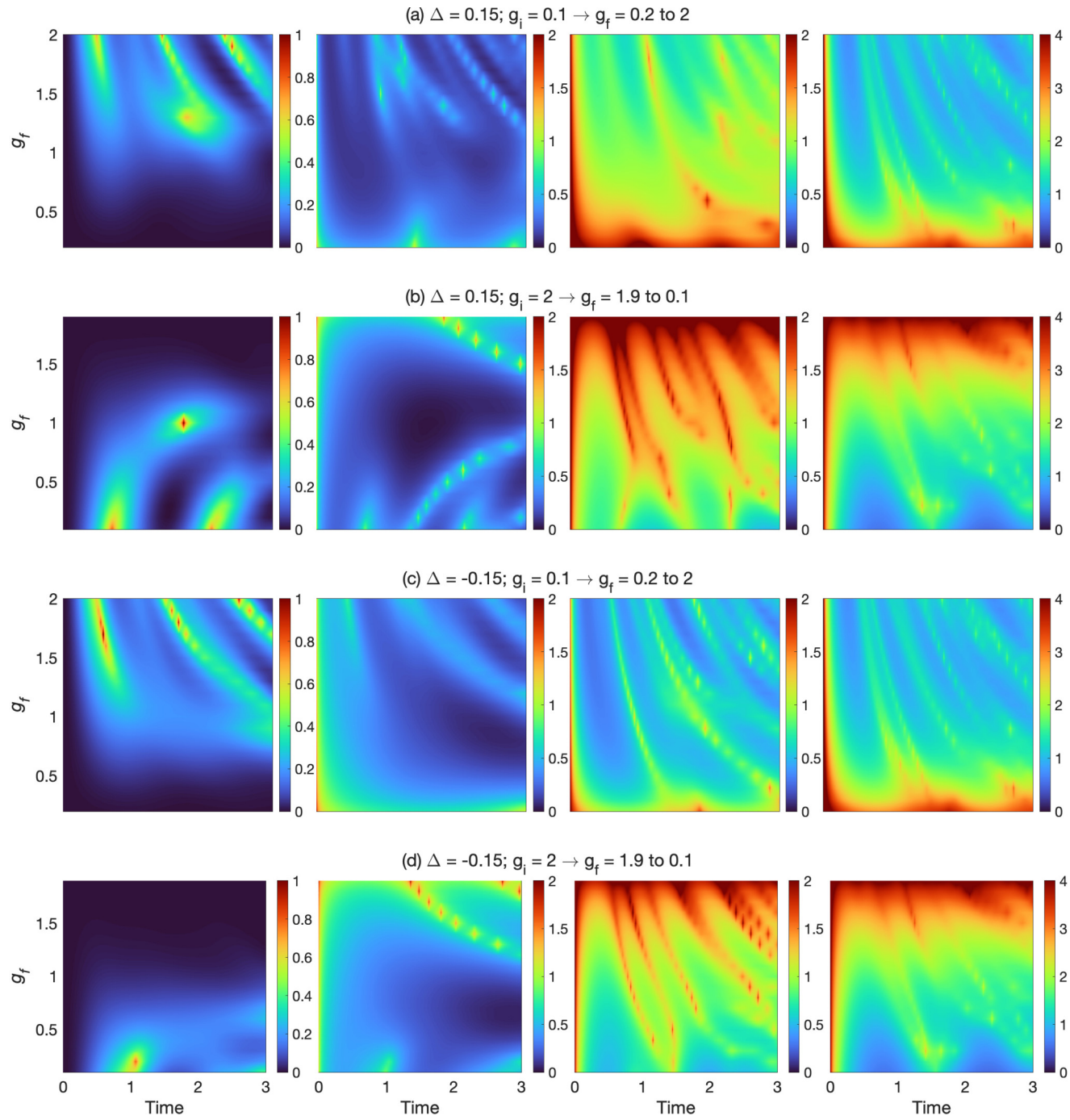

FIG. 6. Same colorplots as Fig. 5 for the ANNNI model. The first two rows represents quench dynamics for positive Δ with forward quench on the top and backward quench on the bottom, while the last two rows show the same setup for negative Δ. Columns starting from the left stand for ground-state, first excited-state, middle energy-state, and highest energy-state LRs, respectively.

of the model consists of four phases—the PM phase, the FM phase, an antiphase (AP) phase with spin configuration of the form $|\uparrow\uparrow\downarrow\downarrow\uparrow\uparrow\cdots\rangle$, and an intermediate floating phase between the PM and the AP phases [38] within the concerned parameter space. In the following, we consider quenching the system between the PM and the FM phase, where the phase boundary for $\Delta < 0$ is given by the equation $1 + 2\Delta = g_c + g_c^2\Delta/[2(1 + \Delta)]$ [38]. We show that the LAS can give insights into the magnetic property of the system.

We first analyze the general quench dynamics for the ANNNI model as we did in the previous section. The same colorplots as for TFIM are displayed in Fig. 6 where the LRS for the ground state, the first excited state, the excited state of energy right in the middle of the spectrum, and the highest excited state are considered for $\Delta = 0.15$ [(a) and (b)] and $\Delta = -0.15$ [(c) and (d)], respectively. From the plots we identify similarities for the two models originating from the same universality class. Note that for a small system size, the excited-state rate functions could behave very differently

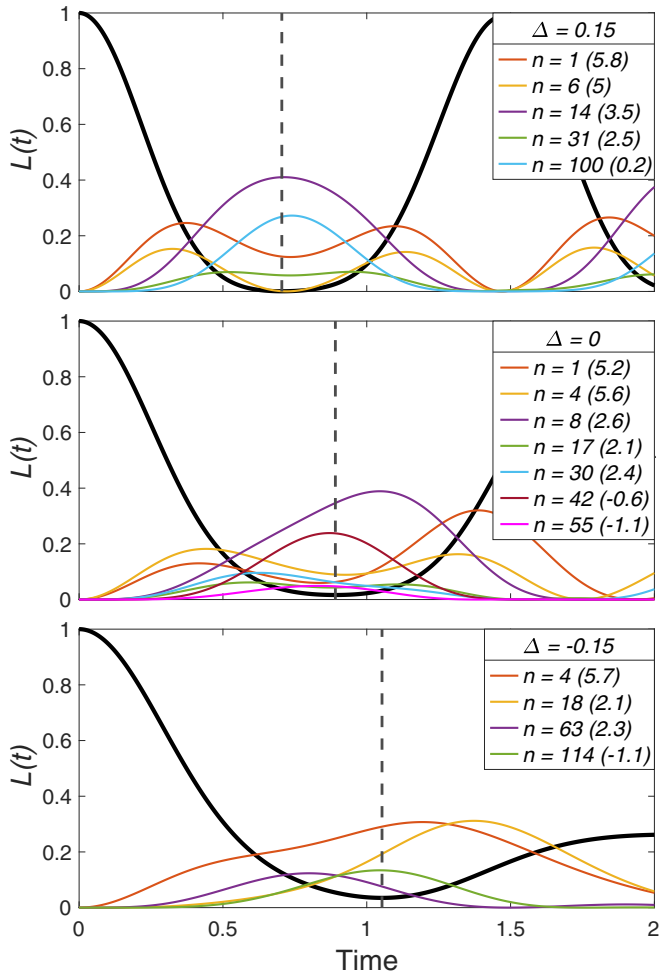

FIG. 7. LES of the quenched $N = 10$ ANNNI model from PM phase to FM phase with $\Delta = 0.15$ (top), $\Delta = 0$ (middle), and $\Delta = -0.15$ (bottom). The black curves correspond to the ground-state LE. The numbers in parentheses refer to the magnetization of each involved excited state. Vertical dashed lines indicate the first critical time when DQPT happens.

among each other compared with those for a larger system size in the case of the Ising model. Nevertheless, the general features can still be seen. The streamlined green peaks for the low-energy states in the first two columns in Fig. 6 approach the corresponding critical points $g_c(\Delta)$ asymptotically for both Δs. As for the higher excited states, the nonanalytical peaks cross the underlying equilibrium phase boundary and the overall magnitudes are higher than those for the lower energy states (last two columns in Fig. 6). The effect of the NNN interaction can also be seen from the plots. Namely, for the LR of the low-energy states, the kinks for negative Δ are less prominent than that of positive Δ [Figs. 6(a) and 6(b)], and the length between two consecutive kinks are slightly longer for negative Δ [Figs. 6(c) and 6(d)] for the reason we will present below. On the other hand, the dynamics start to become ambiguous for higher energy states as seen in the two rightmost columns in Fig. 6.

In the following we explore the physics during DQPT in the ANNNI model by means of LAS. Figure 7 shows LAS in a 10-site system with three different NNN interaction strength

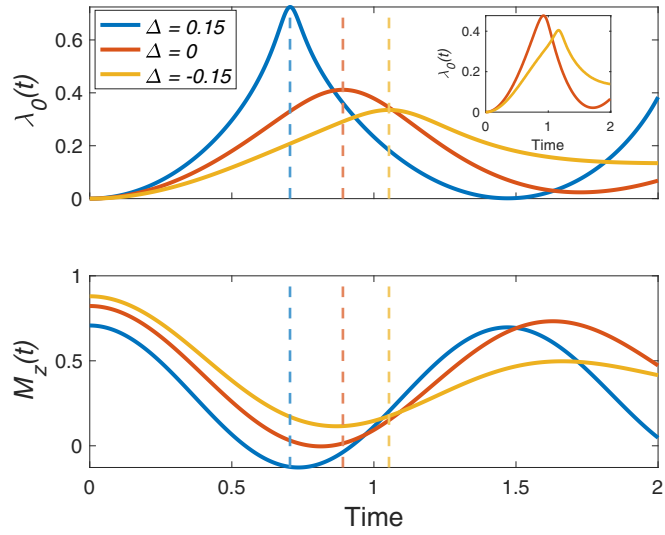

FIG. 8. Quench dynamics and the corresponding time-varying magnetization of the ANNNI model with 10-spin chain. The system is quenched from $g_i = 1.3$ to $g_f = 0.2$ with the corresponding critical times indicated by colored dashed lines. The inset shows the LRs for $\Delta = 0$ and -0.15 for $N = 20$.

Δs: -0.15, 0, and 0.15. The $\Delta = 0$ case refers to the TFIM and is plotted here for comparison. Only the eigenstates with a relatively high contribution in the LAS and their corresponding magnetizations are shown in the figure. Notice that all these highly contributed eigenstates are nondegenerate. From the figure we observe a general DQPT process in the model as follows: For all considered values of Δ, the system is first excited to low-lying excited states followed by an increase of overlap to the higher excited states with lower magnetization in the vicinity of DQPT, and then it relaxes to lower energy states, restoring the high magnetization.

The effect of turning on the NNN interaction causes the system to lean on the eigenstates of weak magnetic character for positive Δ, whereas it hinders the drop of magnetization and even prevents relaxation in the case where Δ is negative, aside from delaying DQPTs. This is the direct consequence of the NNN interaction being negative. The negativity of the interaction introduces a "frustration" on the spins, where the spins "hesitate" whether to align parallel to their nearest spins or antiparallel to their next-nearest neighbors to best minimize energy. This "hesitation" multiplies during dynamical transition where a collective spin flip takes place so that spin flipping for negative Δ is reduced. The immediate effect would be the lesser number of effective states contributing to DQPT than the non-negative Δ cases and a later critical time as seen from Fig. 7.

LAS also reveals some surprising features in the magnetization dynamics. Figure 8 shows the ground-state rate function and the corresponding time-evolving magnetization as given by

$$\langle M_z(t)\rangle = \frac{1}{N}\sum_{j=1}^{N}\left\langle \Psi_i^f(t)\middle|\sigma_j^z\middle|\Psi_i^f(t)\right\rangle, \tag{18}$$

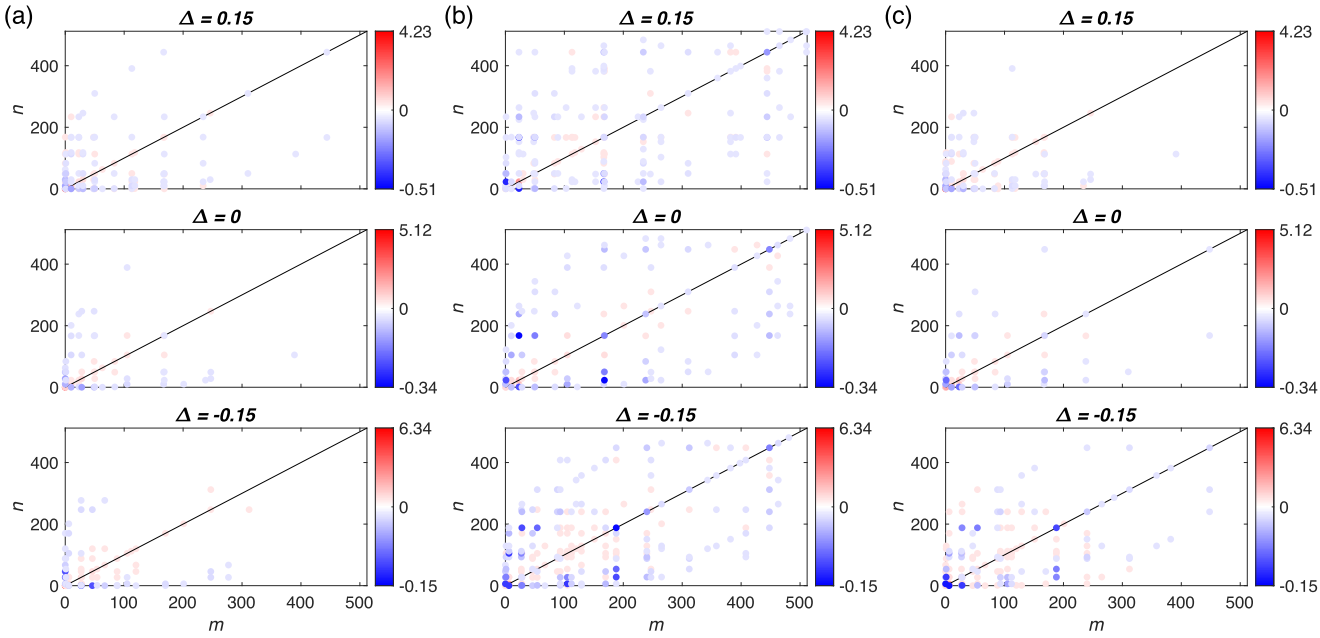

FIG. 9. Explicit values of the term $\mathcal{G}^*_m(t)\mathcal{G}_n(t)\langle\Psi^i_m(0)|\sigma^z_j|\Psi^i_n(0)\rangle$ for the three Δs in three fixed times: (a) Before DQPT, (b) at DQPT, and (c) after DQPT. The quench is done on an $N = 10$ system with quench pair $(g_i, g_f) = (1.3, 0.2)$. The red color represents positive values and blue color represents negative values. Diagonal terms ($m = n$) are highlighted by the diagonal black lines.

where $|\Psi^f_i(t)\rangle = e^{-iH(\Delta,g_f)t}|\psi_0(\Delta, g_i)\rangle$.The peaks in $\lambda_0(t)$ become more prominent as the system size increases (see inset of Fig. 8) and are truly nonanalytic for all Δs showcased in Ref. [38]. Note that each minimum of $\langle M_z(t)\rangle$ does not align strictly with the respective critical times, but qualitative importance can be well illustrated. As Δ increases from a negative value to a positive value, the time difference between the magnetization minimum and the rate function peak reduces. For a positive Δ, the system's magnetization becomes negative in the vicinity of DQPT, whereas it stays positive for a negative Δ.

To understand these, we can express $\langle M_z(t)\rangle$ in Eq. (18) in terms of the LAS as

$$\langle M_z(t)\rangle = \frac{1}{N}\sum_{j=1}^{N}\sum_{m,n}\mathcal{G}^*_m(t)\mathcal{G}_n(t)\langle\Psi^i_m(0)|\sigma^z_j|\Psi^i_n(0)\rangle, \quad (19)$$

where $|\Psi^i_n(0)\rangle = |\psi_n(\Delta, g_i)\rangle$. In a sense, the magnetization is weighted by the spectral behavior of the system. We plotted the individual terms in the summation of Eq. (19) for different Δs at different times in Fig. 9. Only real values are displayed since imaginary parts sum to zero. We observe that the off-diagonal terms of $M_z(t)$ are finite and symmetric along the diagonal as $(\mathcal{G}^*_m(t)\mathcal{G}_n(t))^\dagger = \mathcal{G}^*_n(t)\mathcal{G}_m(t)$, and they have great contribution to the time-evolving magnetization especially at critical time. Obviously σ^z_j does not commute with the Hamiltonian, so σ^z_j is not necessarily diagonal in the initial eigenstate basis. However, since the matrix elements of σ^z_j are fixed, it is the LAS $\mathcal{G}_n(t)$ guaranteeing some particular dynamical structure of the system during dynamical phase transition. Specifically, the "active" off-diagonal terms are the most and most spread out in the spectrum. At DQPT, the system is the most energetic that it would stay in various high-energy states and preferably superposition pairs of eigenstates $[|\psi_m(\Delta, g_i)\rangle, |\psi_n(\Delta, g_i)\rangle]$ in a way to minimize the magnetization in the z direction. Note that most of the contributions come from the superposition pairs, and in the midst of the contributions some pairs give the largest negative values. This is particularly true for positive Δ, where the number of negative terms indicated as blue dots is more and possesses the lowest negative value among the three Δs, as shown in the first plot of Fig. 9(b).

The spectrally weighted magnetization also shows distinguishable features away from critical time. Figures 9(a) and 9(c) captures the instants of $\mathcal{G}^*_m(t)\mathcal{G}_n(t)\langle\Psi^i_m(0)|\sigma^z_j|\Psi^i_n(0)\rangle$ before and after the first DQPT, respectively. In whichever time, the effective terms concentrate on the lower-energy spectrum (lower-left corner of the plots), while the nonzero NNN interaction slightly triggers higher excitations. Similar to the mechanism of DQPT of TFIM, the quench stimulates the system through the lower spectrum, followed by the strongest superimposed state such that those pair states contribute, off-diagonally by calculation, to minimizing magnetization in our studied quench case. After DQPT, the system relaxes to low-lying states as presented by the vanishing of off-diagonal and higher-energy-state terms in Fig. 9(c). Note that the negative Δ case retains some more off-diagonal and higher-half spectrum terms because of the "frustration" explained above.

V. CONCLUSION

In this work, we have introduced the LAS to investigate the physical nature of DQPTs in many-body systems. As examples we studied the LAS and the rate functions on a 1D transverse-field Ising model and a 1D ANNNI model. The former system displays a population redistribution at the vicinity of DQPTs in the momentum space. In particular, the

excitations originally concentrated in the middle range of k values shift to the lower-half range at critical time and relax to the lower levels after the transition. We demonstrated too that LAS plays a role in the evolution of the observables in quenching, for instance, the minimization of transverse magnetization in the study of ANNNI model. From that we infer that at DQPT the system, whether or not frustrated, tends to stay in excited-state pairs in which their combined magnetic property achieves a vanishing or even flipped magnetization.

LAS is a conceptually simple but fundamental analysis method where we directly diagnose the dynamics of the time-evolving systems without the knowledge of the order parameters. This encourages its application to other many-body systems. It is of particular interest to see how LAS emerges in describing physics behind DQPTs for other quantum models, for example, the potential to establish link to order parameters.

ACKNOWLEDGMENTS

We thank Wen-Long You for helpful discussions. This work is financially supported by Research Grants Council of Hong Kong (Grant No. CityU 21304020) and City University of Hong Kong (Grant No. 9610438).

[1] T. Tian, Y. Ke, L. Zhang, S. Lin, Z. Shi, P. Huang, C. Lee, and J. Du, Phys. Rev. B **100**, 024310 (2019).
[2] P. Jurcevic, H. Shen, P. Hauke, C. Maier, T. Brydges, C. Hempel, B. P. Lanyon, M. Heyl, R. Blatt, and C. F. Roos, Phys. Rev. Lett. **119**, 080501 (2017).
[3] J. Zhang, G. Pagano, P. W. Hess, A. Kyprianidis, P. Becker, H. Kaplan, A. V. Gorshkov, Z.-X. Gong, and C. Monroe, Nature (London) **551**, 601 (2017).
[4] N. Fläschner, D. Vogel, M. Tarnowski, B. S. Rem, D.-S. Lühmann, M. Heyl, J. C. Budich, L. Mathey, K. Sengstock, and C. Weitenberg, Nature Phys **14**, 265 (2018).
[5] X.-Y. Guo, C. Yang, Y. Zeng, Y. Peng, H.-K. Li, H. Deng, Y.-R. Jin, S. Chen, D. Zheng, and H. Fan, Phys. Rev. Appl. **11**, 044080 (2019).
[6] M. Heyl, A. Polkovnikov, and S. Kehrein, Phys. Rev. Lett. **110**, 135704 (2013).
[7] P. Titum, J. T. Iosue, J. R. Garrison, A. V. Gorshkov, and Z.-X. Gong, Phys. Rev. Lett. **123**, 115701 (2019).
[8] R. Jafari, Sci. Rep. **9**, 2871 (2019).
[9] M. Schmitt and S. Kehrein, Phys. Rev. B **92**, 075114 (2015).
[10] B. Žunkovič, M. Heyl, M. Knap, and A. Silva, Phys. Rev. Lett. **120**, 130601 (2018).
[11] J. C. Halimeh and V. Zauner-Stauber, Phys. Rev. B **96**, 134427 (2017).
[12] M. Schmitt and M. Heyl, SciPost Phys. **4**, 013 (2018).
[13] G. Torlai, L. Tagliacozzo, and G. D. Chiara, J. Stat. Mech. (2014) P06001.
[14] E. Canovi, E. Ercolessi, P. Naldesi, L. Taddia, and D. Vodola, Phys. Rev. B **89**, 104303 (2014).
[15] M. Heyl, Phys. Rev. Lett. **115**, 140602 (2015).
[16] N. Sedlmayr, P. Jaeger, M. Maiti, and J. Sirker, Phys. Rev. B **97**, 064304 (2018).
[17] S. De Nicola, B. Doyon, and M. J. Bhaseen, J. Stat. Mech. (2020) 013106.
[18] M. Heyl, F. Pollmann, and B. Dóra, Phys. Rev. Lett. **121**, 016801 (2018).
[19] M. Heyl, Phys. Rev. Lett. **113**, 205701 (2014).
[20] J. C. Budich and M. Heyl, Phys. Rev. B **93**, 085416 (2016).
[21] W. C. Yu, P. D. Sacramento, Y. C. Li, and H.-Q. Lin, Phys. Rev. B **104**, 085104 (2021).
[22] T. V. Zache, N. Mueller, J. T. Schneider, F. Jendrzejewski, J. Berges, and P. Hauke, Phys. Rev. Lett. **122**, 050403 (2019).
[23] S. Vajna and B. Dóra, Phys. Rev. B **89**, 161105(R) (2014).
[24] M. Lacki and M. Heyl, Phys. Rev. B **99**, 121107(R) (2019).
[25] A. Lahiri and S. Bera, Phys. Rev. B **99**, 174311 (2019).
[26] K. Yang, L. Zhou, W. Ma, X. Kong, P. Wang, X. Qin, X. Rong, Y. Wang, F. Shi, J. Gong, and J. Du, Phys. Rev. B **100**, 085308 (2019).
[27] A. Kosior and K. Sacha, Phys. Rev. A **97**, 053621 (2018).
[28] T. H. Kyaw, V. M. Bastidas, J. Tangpanitanon, G. Romero, and L. C. Kwek, Phys. Rev. A **101**, 012111 (2020).
[29] A. A. Zvyagin, Phys. Rev. B **95**, 075122 (2017).
[30] R. Jafari, H. Johannesson, A. Langari, and M. A. Martin-Delgado, Phys. Rev. B **99**, 054302 (2019).
[31] R. Jafari and A. Akbari, Phys. Rev. A **103**, 012204 (2021).
[32] S. Zamani, R. Jafari, and A. Langari, Phys. Rev. B **102**, 144306 (2020).
[33] S. Bandyopadhyay, A. Polkovnikov, and A. Dutta, Phys. Rev. Lett. **126**, 200602 (2021).
[34] J. C. Halimeh, D. Trapin, M. VanDamme, and M. Heyl, Phys. Rev. B **104**, 075130 (2021).
[35] A. A. Markov and A. N. Rubtsov, Phys. Rev. B **104**, L081105 (2021).
[36] I. Homrighausen, N. O. Abeling, V. Zauner-Stauber, and J. C. Halimeh, Phys. Rev. B **96**, 104436 (2017).
[37] C. Ding, Phys. Rev. B **102**, 060409(R) (2020).
[38] C. Karrasch and D. Schuricht, Phys. Rev. B **87**, 195104 (2013).
[39] J. N. Kriel, C. Karrasch, and S. Kehrein, Phys. Rev. B **90**, 125106 (2014).
[40] H. Cheraghi, M. J. Tafreshi, and S. Mahdavifar, J. Magn. Magn. Mater. **497**, 166078 (2020).
[41] D. M. Kennes, D. Schuricht, and C. Karrasch, Phys. Rev. B **97**, 184302 (2018).
[42] K. Seetharam, Y. Shchadilova, F. Grusdt, M. B. Zvonarev, and E. Demler, Phys. Rev. Lett. **127**, 185302 (2021).
[43] M. Sadrzadeh, R. Jafari, and A. Langari, Phys. Rev. B **103**, 144305 (2021).
[44] J. Naji, M. Jafari, R. Jafari, and A. Akbari, Phys. Rev. A **105**, 022220 (2022).
[45] R. Jafari, A. Akbari, U. Mishra, and H. Johannesson, Phys. Rev. B **105**, 094311 (2022).
[46] J. C. Halimeh, M. Van Damme, V. Zauner-Stauber, and L. Vanderstraeten, Phys. Rev. Research **2**, 033111 (2020).
[47] T. Hashizume, I. P. McCulloch, and J. C. Halimeh, Phys. Rev. Research **4**, 013250 (2022).
[48] M. Van Damme, T. V. Zache, D. Banerjee, P. Hauke, and J. C. Halimeh, arXiv:2203.01337.

[49] P. Uhrich, N. Defenu, R. Jafari, and J. C. Halimeh, Phys. Rev. B **101**, 245148 (2020).
[50] A. J. Daley, H. Pichler, J. Schachenmayer, and P. Zoller, Phys. Rev. Lett. **109**, 020505 (2012).
[51] S. Hofferberth, I. Lesanovsky, B. Fischer, T. Schumm, and J. Schmiedmayer, Nature (London) **449**, 324 (2007).
[52] P. Richerme, Z.-X. Gong, A. Lee, C. Senko, J. Smith, M. Foss-Feig, S. Michalakis, A. V. Gorshkov, and C. Monroe, Nature (London) **511**, 198 (2014).
[53] S. Choi, J. Choi, R. Landig, G. Kucsko, H. Zhou, J. Isoya, F. Jelezko, S. Onoda, H. Sumiya, V. Khemani, C. V. Keyserlingk, N. Y. Yao, E. Demler, and M. D. Lukin, Nature (London) **543**, 221 (2017).
[54] H. Bernien, S. Schwartz, A. Keesling, H. Levine, A. Omran, H. Pichler, S. Choi, A. S. Zibrov, M. Endres, M. Greiner, V. Vuletić, and M. D. Lukin, Nature (London) **551**, 579 (2017).
[55] E. Guardado-Sanchez, P. T. Brown, D. Mitra, T. Devakul, D. A. Huse, P. Schauss, and W. S. Bakr, Phys. Rev. X **8**, 021069 (2018).
[56] S. Trotzky, Y.-A. Chen, A. Flesch, I. P. McCulloch, U. Schollwöck, J. Eisert, and I. Bloch, Nat. Phys. **8**, 325 (2012).
[57] R. Coldea, D. A. Tennant, E. M. Wheeler, E. Wawrzynska, D. Prabhakaran, M. Telling, K. Habicht, P. Smeibidl, and K. Kiefer, Science **327**, 177 (2010).
[58] P. Jurcevic, B. P. Lanyon, P. Hauke, C. Hempel, P. Zoller, R. Blatt, and C. F. Roos, Nature (London) **511**, 202 (2014).
[59] M. Gring, M. Kuhnert, T. Langen, T. Kitagawa, B. Rauer, M. Schreitl, I. Mazets, D. Adu Smith, E. Demler, and J. Schmiedmayer, Science **337**, 1318 (2012).
[60] B. P. Lanyon, C. Hempel, D. Nigg, M. Müller, R. Gerritsma, F. Zähringer, P. Schindler, J. T. Barreiro, M. Rambach, G. Kirchmair, M. Hennrich, P. Zoller, R. Blatt, and C. F. Roos, Science **334**, 57 (2011).
[61] R. Nandkishore and D. A. Huse, Annu. Rev. Condens. Matter Phys. **6**, 15 (2015).
[62] D. A. Abanin and Z. Papic, Ann. Phys. (Berlin) **529**, 1700169 (2017).
[63] M. Heyl, Rep. Prog. Phys. **81**, 054001 (2018).
[64] A. A. Zvyagin, Low Temp. Phys. **42**, 971 (2016).
[65] E. A. Yuzbashyan, O. Tsyplyatyev, and B. L. Altshuler, Phys. Rev. Lett. **96**, 097005 (2006).
[66] B. Sciolla and G. Biroli, Phys. Rev. Lett. **105**, 220401 (2010).
[67] P. D. Sacramento, Phys. Rev. E **93**, 062117 (2016).
[68] W. C. Yu and S. J. Gu, Chin. Phys. B **25**, 030501 (2016).
[69] M. Serbyn, Z. Papić, and D. A. Abanin, Phys. Rev. X **5**, 041047 (2015).
[70] S. Sachdev, *Quantum Phase Transitions* (Cambridge University Press, Cambridge, England, 1999).
[71] A. Silva, Phys. Rev. Lett. **101**, 120603 (2008).
[72] See Supplemental Material at http://link.aps.org/supplemental/10.1103/PhysRevB.105.174307 for LAS with randomly selected excited states and in the XY model for quench without crossing the equilibrium phase boundary.